

**Nematic fluctuations balancing the zoo of phases in half-filled quantum Hall systems**Andrej Mesáros,<sup>1</sup> Michael J. Lawler,<sup>1,2</sup> and Eun-Ah Kim<sup>1</sup><sup>1</sup>*Laboratory of Atomic and Solid State Physics, Cornell University, Ithaca, New York 14853, USA*<sup>2</sup>*Department of Physics, Applied Physics and Astronomy, Binghamton University, Vestal, New York 13850, USA*

(Received 22 October 2016; revised manuscript received 22 February 2017; published 23 March 2017)

Half-filled Landau levels form a zoo of strongly correlated phases. These include non-Fermi-liquids (NFLs), fractional quantum Hall (FQH) states, nematic phases, and FQH nematic phases. This diversity begs the following question: what keeps the balance between the seemingly unrelated phases? The answer is elusive because the Halperin-Lee-Read description that offers a natural departure point is inherently strongly coupled. However, the observed nematic phases suggest that nematic fluctuations play an important role. To study this possibility, we apply a recently formulated controlled double-expansion approach in large- $N$  composite fermion flavors and small  $\epsilon$  nonanalytic bosonic action to the case with both gauge and nematic boson fluctuations. In the vicinity of a nematic quantum critical line, we find that depending on the amount of screening of the gauge- and nematic-mediated interactions controlled by  $\epsilon$ 's, the renormalization-group flow points to all four mentioned correlated phases. When pairing preempts the nematic phase, NFL behavior is possible at temperatures above the pairing transition. We conclude by discussing measurements at low tilt angles, which could reveal the stabilization of the FQH phase by nematic fluctuations.

DOI: [10.1103/PhysRevB.95.125127](https://doi.org/10.1103/PhysRevB.95.125127)**I. INTRODUCTION**

The complexity of a phase diagram is a hallmark of strongly correlated systems, and it represents the rich physics of correlation. It also challenges theoretical progress by making it hard for one to decide on the minimal model that will nevertheless faithfully represent the system of interest. Interestingly, upon a simple change of filling tuned by a magnetic field, half-filled Landau levels switch through a zoo of exotic states that are commonly observed among strongly correlated materials. Specifically, the  $\nu = 1/2$  state is one of the best established non-Fermi-liquid states [1–4], the  $\nu = 5/2$  state is the strongest candidate for a non-Abelian fractional quantum Hall state [5–10] with  $p + ip$  channel pairing of composite fermions [11,12], and the  $\nu = 9/2$  state is an electronic nematic state [13–15]. More recently, the  $\nu = 1/2$  state also attracted intense interest among the theory community [16–18] as a possible gate into correlated topological surface states.

Indeed, the zoo of complex phases in the quantum Hall phase diagram has attracted many authors to view it as a paradigmatic place to explore quantum complexity [19–27]. Nevertheless, understanding the interplay of correlated states through a unified description remains an open question. In particular, the question of the mechanism of pairing in the fractional quantum Hall state remains open despite intense efforts and interest in the community [28]. The clearest indication about pairing comes from numerical studies of interacting electrons in the  $\nu = 5/2$  ground state [29–31]. Unfortunately, a theoretical understanding remains elusive, since fluctuations of the internal gauge field prevent the  $p + ip$  pairing of composite fermions in the half-filled Landau-level systems [1,32–35].

Nematic fluctuations provide a clue to the question of pairing. Phenomenologically, not only does the FQH  $\nu = 5/2$  state give way to a nematic state with the gap closing under an in-plane field [14,36,37], it also exhibits transport anisotropy before the gap closes [19,38,39]. In particular, a recent

observation of the transition between the FQH  $\nu = 5/2$  state and a nematic induced by isotropic pressure [40] is a striking demonstration of the proximity between the nematic state and the FQH  $\nu = 5/2$  state. Interestingly, recently a number of theoretical works have been establishing the idea that nematic fluctuations can enhance pairing [41–46]. Nevertheless, little attention has been given to the role of putative nematic quantum critical fluctuations in forming the FQH  $\nu = 5/2$  state to date. Here we study the role of nematic quantum critical fluctuations in the pairing of composite fermions assuming that a nematic quantum critical point can be accessed through a tuning parameter such as isotropic pressure (see Fig. 1). Moreover, as it is known that the filled Landau levels change the effective interactions [47], we envision a measure of dominance of nematic fluctuation to change with the changing of the Landau level (parametrized by  $\delta$  in Fig. 1). Hence we have a schematic phase space of Fig. 1 in mind, where the quantum critical value of pressure  $p_c$  is changing with  $\delta$  and defining a quantum critical line.

Specifically, we build on the recent progress in addressing the challenging problem of a Fermi surface coupled to massless fluctuations through a controlled perturbative renormalization-group (RG) double expansion [42,48], and we investigate the instabilities in systems in which both nematic and gauge fluctuations are present.

The rest of the paper is organized as follows: In Sec. II we introduce the model and details of the RG procedure. Section III considers the resulting states, pairing, and non-Fermi-liquid behaviors at the nematic quantum critical line (NQCL). Behavior that is removed slightly from the NQCL is considered in Sec. IV. We close with a discussion of the applicability of our work, and a summary of the results and experimental predictions.

**II. MODEL**

To study the interplay between nematic quantum critical fluctuations and gauge fluctuations [1] in half-filled Landau

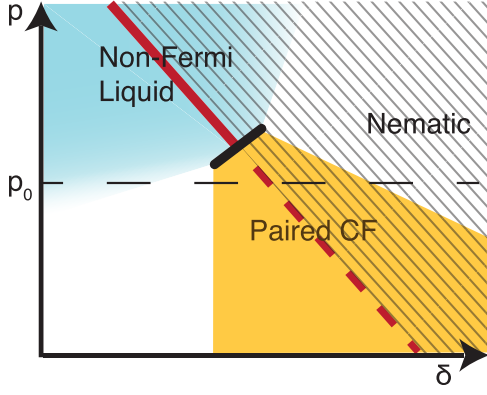


FIG. 1. Phase diagram in the vicinity of a quantum nematic transition occurring at critical isotropic pressure  $p_c(\delta)$  (red line) as a function of a measure  $\delta$  of dominance of nematic-mediated over gauge-mediated bare interactions. The hatched region is nematically ordered. Along the dashed red line, the nematic transition is preempted by a paired (composite) fermion state (orange). At ambient pressure ( $p_0$ ), a non-Fermi-liquid (blue) and gapless nematic (gray on right) are also present. A continuous pairing transition occurs on the black line.

levels, we extend the model in Ref. [48]. As in Ref. [48], we consider  $N$  species of fermions and break up the Fermi surface of each species into independent patches [49], i.e., we decompose the  $a$ th composite fermion field  $\psi^a(\tau, r)$  in two spatial dimensions  $r$  and imaginary time  $\tau$  with  $a = 1, \dots, N$  into patch fields, i.e.,

$$\psi^a(\tau, r) = \sum_{j,s} \psi_j^{s,a}(\tau, r) e^{isk_j r}, \quad (1)$$

where the  $j$ th patch pair is located at opposite Fermi momenta  $sk_j$ ,  $s = \pm 1$  [see Fig. 2(a)], assuming an inversion-symmetric Fermi surface. For every patch pair  $j$ , we align the  $x$  axis with  $k_j$  and define the patches by  $|k_x| < \Lambda_x$ ,  $|k_y| < \Lambda_y$ . The action

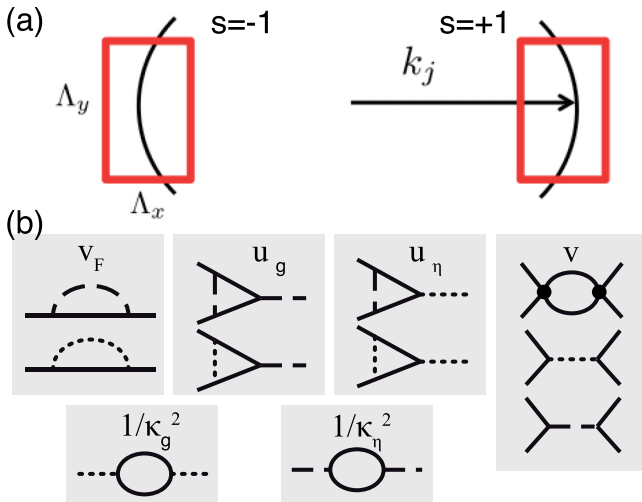


FIG. 2. Model and RG scheme. (a) Patch pair  $j$ , with corresponding Fermi momenta  $\pm k_j$ . (b) One-loop diagrams contributing to the flow of coupling constants, with a fermion propagator (full line), a nematic propagator (dashed), a gauge field propagator (dotted), and four-fermion interaction (dot).

for the patch fermions is then given by

$$S_j^f = \sum_{k,s,a} \bar{\psi}_j^{s,a}(k) D_s(k) \psi_j^{s,a}(k), \quad (2)$$

where  $D_s(k) \equiv -i\omega_k + v_F(sk_x + \frac{1}{2K}k_y^2)$  and  $v_F$  is the Fermi velocity,  $K$  is the local Fermi surface curvature, and  $k \equiv (\omega_f, k_x, k_y)$  represent the fermionic Matsubara frequency  $\omega_f$  and the patch momenta, while the normalized sum is  $\sum_k \equiv \frac{1}{\beta} \sum_{\omega_f} \int \frac{d^2k}{(2\pi)^2}$ .

Reference [48] considered fermions coupled to a single boson, controlling the RG expansion using two small parameters:  $1/N$  and the deviation [50] of the boson's dynamic critical exponent from 2. For composite fermions coupled to nematic quantum critical fluctuations, our fermions on the patch pair  $j$  will be each coupled to two bosonic fields: the massless transverse component (in the direction of Fermi momentum, see Appendix A) of the gauge field [49],  $\phi_g(\tau, r)$ , and the nematic fluctuation,  $\phi_\eta(\tau, r)$ , which is massless at the NQCL. We then follow Ref. [42] and break the nematic and gauge fields into separate patch fields [41,49]  $\phi_{j,\eta}(\tau, r)$  and  $\phi_{j,g}(\tau, r)$ . The bosonic action is then

$$S_j^b = \frac{1}{2\kappa_\eta^2} \sum_q |q_y|^{1+\epsilon_\eta} |\phi_{j,\eta}(q)|^2 + \frac{r_0}{2} \sum_q |\phi_{j,\eta}(q)|^2 + \frac{1}{2\kappa_g^2} \sum_q |q_y|^{1+\epsilon_g} |\phi_{j,g}(q)|^2 + \dots \quad (3)$$

with  $q \equiv (\omega_b, q_x, q_y)$  the bosonic Matsubara frequency and momentum variables, the bare mass  $r_0$  measures the distance to the NQCL from either side of the transition, and “...” represent all other irrelevant analytic terms that we will ignore. Here  $\kappa_\eta$  and  $\kappa_g$ , the boson couplings for the nematic and gauge boson, respectively, get renormalized under RG [see Fig. 2(b)]. We retain control of the calculation for small enough nematic mass (see Appendix F), in a regime of strong fermion-nematic coupling that is complementary to the one accessed by Ref. [43]. The deviation of each boson's dynamic critical exponents from 2 represented by  $\epsilon_\eta < 1$  for the nematic fluctuation and  $\epsilon_g < 1$  for the gauge boson will control two double expansions together with  $1/N$ . Due to the nonanalyticities in the action, these will not renormalize under RG [48]. Further, we will treat  $\epsilon_\eta$  and  $\epsilon_g$  as phenomenological parameters rather than view any particular value as “physical.” When coupled to fermions, these bosons mediate interaction between fermions. As filled Landau levels change the effective interaction between composite fermions [51], in effect we anticipate the bare values of  $\epsilon_\eta$  and  $\epsilon_g$  to vary with the number of filled Landau levels and other external controls such as pressure.

All together, the full effective action  $S_j$  for each patch pair  $j$  is

$$S_j = S_j^f + S_j^b + S_j^{\text{int}}, \quad (4)$$

where  $S_j^{\text{int}}$  represents the coupling between bosons and fermions,

$$S_j^{\text{int}} = \frac{u_\eta}{\sqrt{N}} \sum_{k,q} \phi_{j,\eta}(q) \sum_{s,a} \bar{\psi}_j^{s,a}(k+q) \psi_j^{s,a}(k) + \frac{u_g}{\sqrt{N}} \sum_{k,q} \phi_{j,g}(q) \sum_{s,a} s \bar{\psi}_j^{s,a}(k+q) \psi_j^{s,a}(k), \quad (5)$$

with coupling constants  $u_\eta$  and  $u_g$  for the nematic-fermion and gauge-fermion interaction, respectively, being renormalized under the RG [Fig. 2(b)]. Note the difference in the sign of the coupling [33]: the nematic field couples to the density, and hence the coupling is independent of the patch label. Contrastingly, the gauge field couples to the current and hence the coupling has opposite signs on the two patches  $s = \pm 1$ .

Finally, our main goal is to investigate how the two critical couplings affect pairing of the composite fermions leading to the  $\nu = 5/2$  state. For this we analyze fermion pairing instabilities by considering the residual composite fermion interaction in the BCS channel,

$$S^{\text{BCS}} = -\frac{1}{4} \sum_{k,k',a} V^{\alpha\beta\gamma\delta}(k-k') \bar{\psi}_\alpha^a(k) \bar{\psi}_\beta^a(-k) \psi_\gamma^a(k') \psi_\delta^a(-k'), \quad (6)$$

where we explicate spin indices, and we use that in a rotationally invariant system (true near enough to the NQCL) the interaction depends only on the angle of  $q = k - k'$  with momenta  $k$  and  $k'$  taken on the Fermi surface. We consider the  $S^{\text{BCS}}$  term without expanding in patch fermion species for efficiency. Interpatch interactions it contains get renormalized when high-momentum bosons are integrated out, and this form enables us to ignore the details of the patching procedure [Fig. 2(b) and Ref. [42]].

### III. RG FLOW AND PHASE DIAGRAM ON THE NQCL

Within the perturbative RG approach, we consider the NQCL Gaussian theory and the free-fermion fixed point, working in the zero-temperature limit at the NQCL. The scaling that preserves the functional form of the fermionic propagator [Eq. (2)] is

$$k_x \rightarrow tk_x, \quad k_y \rightarrow t^{1/2}k_y, \quad \omega \rightarrow t\omega, \quad (7)$$

with  $t = e^{-l}$ , and  $l$  being the RG scale. We set the same scalings for bosonic variables. To define the fermionic and bosonic modes to be integrated out, for every patch pair located at  $\pm k_j$  we align the  $x$  axis with  $k_j$ , fixing the patches as  $|k_x| < \Lambda_x$ ,  $|k_y| < \Lambda_y$ , and then we choose the high-energy fermion modes at  $t\Lambda_x < |k_x| < \Lambda_x$  and bosonic ones at  $\sqrt{t}\Lambda_y < |q_y| < \Lambda_y$ . The fermionic modes at  $\sqrt{t}\Lambda_y < |k_y| < \Lambda_y$  cross the Fermi surface and cannot be integrated out, so to preserve the patch aspect ratio with each RG step we relegate these modes to new patches.

The above RG method introduced in Ref. [42] is a hybrid between a two-patch scheme that focuses on interactions within a patch, and a multipatch scheme that focuses on interpatch interactions. It merges the two schemes by being agnostic about how new patches are introduced at each RG step. As such, the method does not track information about the geometry of the Fermi surface. Although recent findings on the importance of Fermi surface geometry were limited to Fermi surfaces in higher dimensions [52], the lack of a systematic scheme for introducing new patches may still harbor problems. Nevertheless, we proceed here assuming that there exists at least one well-defined way to introduce new patches at each RG step.

The total action in Eq. (4) has two dimensionless couplings at the NQCL: a fermion-gauge coupling constant and a

fermion-nematic coupling constant, i.e.,

$$g = \frac{u_g^2 \kappa_g^2}{(2\pi)^2 v_F \Lambda_y^{\epsilon_g}}, \quad \eta = \frac{u_\eta^2 \kappa_\eta^2}{(2\pi)^2 v_F \Lambda_y^{\epsilon_\eta}}, \quad (8)$$

respectively. Both couplings are relevant at our initial fixed point (Gaussian nematic and free fermion). For the BCS instability, the coupling constants in Eq. (6),  $V^{\alpha\beta\gamma\delta}(k-k')$ , in all spin-symmetric or spin-antisymmetric channels with fixed angular momentum are rendered indistinguishable within one-loop RG and hence may be labeled by a single constant  $V$ . The corresponding dimensionless coupling constant is

$$v = \frac{k_F}{2\pi v_F} V, \quad (9)$$

where  $v < 0$  ( $v > 0$ ) is attraction (repulsion).

One-loop quantum corrections in our RG [see Fig. 2(b)] give the following flow equations for the Cooper pairing:

$$\frac{dv(l)}{dl} = -v(l)^2 - f(l), \quad f(l) \equiv \eta(l) - g(l), \quad (10)$$

where we introduced the running coupling  $f(l)$  to keep track of the competition between nematic and gauge fluctuations. Positive  $f$  promotes attraction in the BCS channel, and negative  $f$  suppresses it. Interestingly, within our theory not only can  $f(l)$  have either sign but its sign can change during the RG flow. The remaining couplings flow as

$$\begin{aligned} \dot{g} &= g \left( \frac{\epsilon_g}{2} - \frac{\eta}{N} - \frac{g}{N} \right), \quad \dot{\eta} = \eta \left( \frac{\epsilon_\eta}{2} - \frac{\eta}{N} - \frac{g}{N} \right), \\ \dot{v}_F &= -v_F \left( \frac{\eta}{N} + \frac{g}{N} \right), \end{aligned} \quad (11)$$

where an explicit  $l$  dependence is dropped. The last equation shows that coupling to both of the bosons enhances the tendency toward a non-Fermi-liquid state, which is characterized by a vanishing Fermi velocity  $v_F$ . Note that the local four-fermion interactions (in any particle-hole channel as well as in the BCS channel) do not influence the flow of boson-fermion couplings at the one-loop level. This is because all pertinent diagrams vanish due to the vanishing of the fermion polarization bubble. Such vanishing of the polarization bubble was already reported in Ref. [48]. One can also understand this absence of a ‘‘backreaction’’ by considering the four-fermion term induced by a boson-fermion coupling (5) when the boson is integrated out. The induced four-fermion term has a factor  $\sim 1/|k|^{1+\epsilon}$  coming from the boson propagator, making it more relevant than a corresponding local interaction term.

The two RG equations for the fermion-boson couplings  $g, \eta$  in Eq. (11) do not involve other couplings, so we start from the  $g, \eta$  plane in which there are obvious fixed points: Beside the unstable free point  $(g, \eta) = (0, 0)$ , there are  $(g, \eta) = (g_*, 0)$  and  $(g, \eta) = (0, \eta_*)$ , where the defined numbers

$$g_* \equiv \frac{N\epsilon_g}{2}, \quad \eta_* \equiv \frac{N\epsilon_\eta}{2} \quad (12)$$

can take finite values in the double expansion  $\epsilon_g, \epsilon_\eta \rightarrow 0$ ,  $N \rightarrow \infty$ . As the existence of fixed points is established, for simplicity in the following we set  $N = 1$  and consider the  $g_*, \eta_* \ll 1$  limit. In our approach, different experimental circumstances correspond to different bare values of running couplings  $\eta_0$  and  $g_0$ , as well as to the balance between  $\eta_*$  and  $g_*$  (i.e.,  $\epsilon_\eta$  and  $\epsilon_g$ , respectively). Since we take the physical value

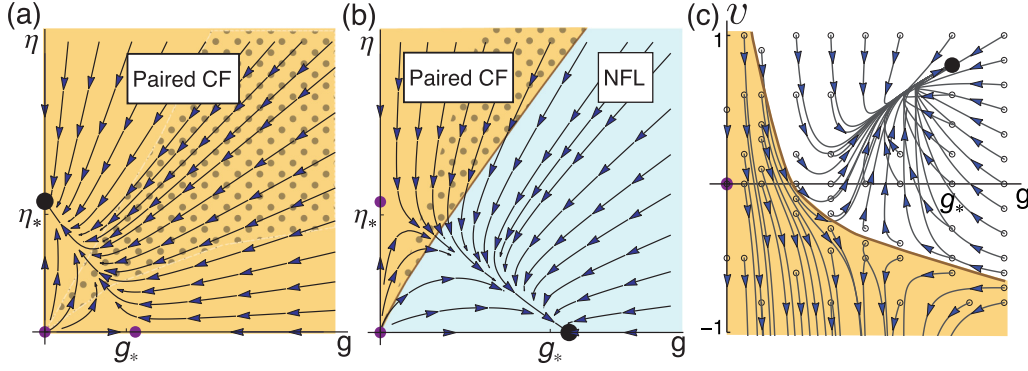


FIG. 3. RG flows at the NQCL projected onto planes in space of fermion-gauge ( $g$ ), fermion-nematic ( $\eta$ ), and pairing interaction ( $v$ ) couplings. Fixed points, stable (large dot), or unstable (small dot) in the plane are marked. (a,b) In the orange region, the (composite) fermions pair with vanishing bare attraction, i.e., a gapped FQH is formed. (a) The value  $g_*/\eta_* = 0.7$  is representative for all  $\epsilon_g < \epsilon_\eta$ . In the dotted orange area, the NFL energy scale is higher than the pairing gap scale. (b) The choice  $g_*/\eta_* = 1.44$  is representative for all  $\epsilon_g > \epsilon_\eta$ . The  $(g_*, 0)$  point is isotropic NFL (blue). At the boundary between the regions, the pairing energy scale becomes zero. This phase diagram is robust away from the nematic quantum critical line (see Fig. 8). (c) Pairing instability for initial repulsion ( $v > 0$ ) or attraction ( $v < 0$ ), with  $g_*/\eta_* = 1.44$  as in (b) and the choice  $\eta_0 = 0.67\eta_*$ . The stable NFL fixed point  $(g, \eta, v) = (g_*, 0, v_*)$  is given by  $v_* = \sqrt{g_*} = 0.8$  [see Eq. (C3)]. Flows starting in the orange region show pairing instability since  $v \rightarrow -\infty$  at a finite RG scale.

of bare pairing to be  $v_0 = 0$ , the pairing instabilities as well as the non-Fermi-liquid behavior are then fully determined by the values of  $\eta_0, g_0, \eta_*, g_*$ . The fine-tuned case  $\epsilon_g = \epsilon_\eta$  is exceptional, and it exhibits a line of fixed points connecting the two fixed points  $(g_*, 0)$  and  $(0, \eta_*)$  at the one-loop level (see Appendix B). As the RG flows of  $(g, \eta)$  and especially of the pairing coupling constant  $v$  qualitatively differ depending on which one of the  $\epsilon_g, \epsilon_\eta$  is larger, we analyze the two cases separately. For each case, we infer the possible phases assuming that the bare values of the fermion-boson couplings  $(g_0, \eta_0)$  represent different experimental circumstances.

In the case  $\epsilon_g < \epsilon_\eta$  with the dynamic critical exponent of the nematic boson being larger, the only stable fixed point in the  $(g, \eta)$  plane is  $(g, \eta) = (0, \eta_*)$  [see Fig. 3(a)]. Obviously, the fermions always pair (except when  $\eta_0 = 0$  exactly), because  $f(l)$  [see Eq. (10)] here flows from the value  $\eta_0 - g_0$  to  $\eta_* > 0$ . Therefore, eventually  $f(l)$  turns positive and stays that way, giving a pairing instability even with  $v_0 = 0$  to realize a gapped FQH state. A remarkable consequence of this result is that the paired state is realized even in the limit in which the bare coupling of the fermions to the gauge fluctuations dominates over the bare coupling to the nematic fluctuations. Gauge fluctuations are no longer impeding pairing enough to push it to require a finite attractive interaction. Instead they only suppress the value of the pairing (FQH) gap estimated as  $\Delta_P \sim \exp(-l_P)$  when a pairing instability  $v = -\infty$  develops at a finite RG scale  $l_P$ . In the most extreme case of  $g_0 \rightarrow \infty, \eta_0 \rightarrow 0$ , we obtained an analytic expression for the suppressed pairing gap in the limit  $\eta_* - g_* \ll g_*$  to be (see Appendix C)

$$\Delta_P \sim \left(\frac{\eta_0}{g_0}\right)^{1/(\eta_* - g_*)} \exp(-\pi/\sqrt{\eta_*}). \quad (13)$$

Although the NFL dictated by vanishing Fermi velocity in Eq. (11) is unstable to infinitesimal pairing in the entire phase space of  $(g_0, \eta_0)$  in this case, the NFL effects may be visible at temperatures above pairing  $T_c$ . This requires the energy scale associated with the NFL to be larger than the pairing gap

scale, which occurs in the dotted region of Fig. 3(a) dictated by sufficiently large  $(g_0 + \eta_0)$  (see Appendix E).

In the case  $\epsilon_g > \epsilon_\eta$  with the dynamic critical exponent of the gauge boson being larger, there is a richer set of possibilities [see Fig. 3(b)]. Namely, depending on the two bare boson-fermion coupling strengths, we find either a stable non-Fermi-liquid [blue region in Fig. 3(b)] or a paired state [orange in Fig. 3(b)]. Moreover, we find that the two phases in the  $(g_0, \eta_0)$  plane are separated by a continuous phase transition at the phase boundary given by

$$(\eta_0 - g_0) \ln\left(\frac{\eta_0}{g_0}\right) = (g_* - \eta_*)\sqrt{g_*} \quad (14)$$

for  $g_* - \eta_* \ll g_*$ . Although the phase boundary in Fig. 3(b) needs to be obtained numerically in general (see Appendix D), a simple intuition can be gleaned from the  $\beta$  function in Eq. (10). When  $g_0 > \eta_0$ , the function  $f(l)$  stays negative throughout the RG flow and pairing requires above-threshold strength of the attractive bare interaction. Therefore, the fixed point  $(g_*, 0)$  controls the blue region of Fig. 3(b). As Eq. (11) dictates, the Fermi velocity  $v_F$  flows to zero in this region, resulting in a NFL phase driven by gauge fluctuations as in the original HLR model [1, 50]. On the other hand, pairing can occur as an infinitesimal instability for  $g_0 \ll \eta_0$  despite  $(g_*, 0)$  being the only stable fixed point. This is because  $f(l)$  starts off positive for these bare values of couplings, and the pairing instability can take over before  $f(l)$  eventually turns negative. In fact, for  $g_0$  sufficiently smaller than  $\eta_0$ , the pairing instability occurs even if the initial coupling in the BCS channel [Eq. (9)] is repulsive,  $v > 0$ ; see Fig. 3(c). The NFL effects may be visible again in the dotted region of the paired state [see Fig. 3(b) and after Eq. (13)]. Furthermore, the continuity of the transition is evident by the fact that the pairing gap of the infinitesimal instability vanishes as  $(g_0, \eta_0)$  approaches the phase boundary of Eq. (14) with an analytic form we find for  $g_* - \eta_* \ll g_*$ ,

$$\Delta_P \sim x^{\frac{1}{2\sqrt{g_*}}} \left(\frac{g_0}{\eta_0}\right)^{1/\delta_*}, \quad (15)$$

where  $x$  parametrizes a small distance in  $(g_0, \eta_0)$  from the phase boundary (see Appendix D).

Overall we established that a composite fermion system tuned to the NQCL can be in one of two ground states: a paired state promoted by nematic fluctuations (orange regions in Fig. 3) or a stable NFL state governed by the gauge fluctuations [blue region in Fig. 3(b)]. If we associate the paired CF state with the  $\nu = 5/2$  FQH state, our model indicates that pairing in the  $\nu = 5/2$  FQH state is driven by the nematic fluctuations. Further associating the NFL state with the  $\nu = 1/2$  NFL state, we are invited to postulate the influence of nematic fluctuation to be weaker at lower Landau levels. If the degree of dominance between the two gapless bosons is varied with experimental conditions and the filling factor, and further the distance to the nematic phase can be varied with an external control such as isotropic pressure, we can now divide the NQCL into two parts as in Fig. 1.

#### IV. PHASES IN THE VICINITY OF THE NQCL

Because accessing the quantum NQCL would require fine tuning, we now consider the effect of finite distance from the NQCL with finite  $r_0$  in Eq. (3). The positive mass  $r_0 > 0$  will leave the system in the isotropic phase. But negative mass  $r_0 < 0$  will drive the system into a nematic phase where the nematic order parameter gains a finite expectation value. However, the analysis of the fluctuation around this expectation value will closely follow the analysis of the nematic fluctuation in the isotropic phase. From hereon we refer to the dimensionless coupling associated with the quadratic term in the action for the nematic fluctuation as  $R$ , which is always relevant. Moreover, a runaway flow of the nematic-fermion coupling  $\eta$  takes the system to a strong-coupling regime outside the applicability of our methods when  $\epsilon_g < \epsilon_\eta$ . Nevertheless, we can study the regime near the NQCL by cutting the RG flows when  $R$  reaches some limiting value.

The nematic mass generally weakens the influence of nematic fluctuations, and the RG equations now become

$$f(l) \equiv \frac{\eta(l)}{1 + R(l)} - g(l) \quad (16)$$

and

$$\begin{aligned} \dot{g} &= g \left( \frac{\epsilon_g}{2} - \frac{\eta}{N} \frac{1}{1 + R} - \frac{g}{N} \right), \\ \dot{\eta} &= \eta \left( \frac{\epsilon_\eta}{2} - \frac{\eta}{N} \frac{1}{1 + R} - \frac{g}{N} \right), \\ \dot{v}_F &= -v_F \left( \frac{\eta}{N} \frac{1}{1 + R} + \frac{g}{N} \right). \end{aligned} \quad (17)$$

Again we can establish a phase boundary between a paired state and a NFL state in the  $(\eta_0, g_0)$  phase diagram (see Appendix F). In the region of bare couplings where  $\eta_0$  is sufficiently larger than  $g_0$ , the  $f(l)$  starts out positive. If pairing instability takes over before  $R(l)$  grows substantially, the system will end up in a paired state. On the other hand, when  $\eta_0 \ll g_0$ ,  $f(l)$  starts off negative and ultimately the rapid growth of  $R$  ensures  $f(l) \rightarrow -g_*$  as  $l \rightarrow \infty$  leaving the system controlled by the gauge fluctuation without pairing. Now depending on the sign of  $r_0$ , the paired state and the NFL state each may be isotropic

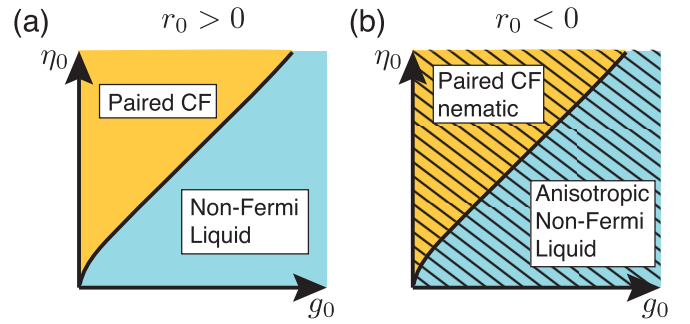


FIG. 4. Phases realized for different bare fermion-gauge ( $g_0$ ) and fermion-nematic ( $\eta_0$ ) couplings when the system is in the vicinity of the nematic quantum transition. (a) In the disordered phase with positive nematic mass  $r_0 > 0$ , either a NFL (blue) or a paired state (orange). (b) In the nematically ordered phase with negative nematic mass  $r_0 < 0$ , either an anisotropic NFL (shaded blue) or a gapped paired nematic state (shaded orange).

or nematic. Hence one can anticipate phase diagrams in Fig. 4 with four distinct phases: isotropic paired CF, isotropic NFL [Fig. 4(a)], nematic paired CF, and nematic NFL [Fig. 4(b)]. Indeed, a systematic study of RG flows conforms to this anticipation (see Appendix F). Hence within the regime of validity of our approaches, we see that the observation of a nematic fluctuation driven pairing phase and a stable NFL phase we obtained at the NQCL survives moving away from the NQCL line. The new facets introduced by considering the nematically ordered phase are the possibilities of having an anisotropic paired state and anisotropic NFL state (see Fig. 1).

#### V. DISCUSSION AND CONCLUSIONS

To summarize, we used double expansion [48] in boson dynamic exponents [50] and number of fermion species [49] to study the NQCL and its vicinity in composite Fermi fluid. This approach has several issues, including the fact that it relies on nonanalytic bosonic actions and an incompletely specified RG prescription. Nevertheless, we found the interplay between gauge fluctuations and nematic fluctuations to account for the entire zoo of correlated states observed in half-filled Landau levels. To start with, we capture the NFL state at  $\nu = 1/2$ , the FQH state at  $\nu = 5/2$  (paired CF state), and the gapless nematic state at  $\nu = 9/2$ . Moreover, the gapped FQH nematic observed in a tilted field experiment [39] naturally appears on the nematic ordered side of the NQCL with the pairing driven by nematic fluctuation. Finally, a recent observation of the transition between a FQH state and a nematic state driven by isotropic pressure suggests that the NQCL we envision in Fig. 1 can be accessed using pressure [40].

There are several other intriguing correlated states that we left out in this study. It is plausible that striped states, such as a recently proposed particle-hole symmetric liquid [53], could be described by a  $2k_F$  instability of an extended theory. However, such an instability in a two-patch theory is likely to be dominated by the pairing instability without nesting [48]. Another interesting question concerns the competition between a Moore-Read Pfaffian state [11,12] and its particle-hole-conjugate anti-Pfaffian state [54], with each of

these conjectured states corresponding to different pairing symmetry channels of CFs. Unfortunately with our minimal number of patches, we cannot distinguish different pairing channels. Nevertheless, an extension of our work, including a larger number of patches, may be useful in studying the competition between Pfaffian and anti-Pfaffian states, and it may even include a striped Pfaffian–anti-Pfaffian phase [55].

The key insight that emerges from our result is that the pairing of CFs in  $\nu = 5/2$  systems can be driven by nematic fluctuations in the vicinity of the NQCL. Therefore, we predict the magnitude of the FQH gap in  $\nu = 5/2$  to be correlated with the nematic fluctuations, which can be quantified through measuring nematic susceptibility. To achieve this, one possibility is to measure the nematic susceptibility in  $\nu = 5/2$  states by studying nematicity as a function of small tilt-angles. Then our results predict the nematic susceptibility so-measured to be monotonically correlated with the size of the FQH gap at zero tilt-angle.

### ACKNOWLEDGMENTS

We thank Jim Eisenstein, Eduardo Fradkin, Michael Manfra, David Mross, Michael Mulligan, and Senthil Todadri for helpful discussions. A.M. and E-A.K. are supported by the U.S. Department of Energy, Office of Basic Energy Sciences, Division of Materials Science and Engineering under Award No. DE-SC0010313. E-A.K. acknowledges support through the Simons Fellowship for Theoretical Physics. E-A.K. and M.J.L. are grateful for the hospitality of KITP during the completion of this work.

### APPENDIX A: FROM THE HLR GAUGE FIELD TO A SCALAR FIELD

We briefly review the HLR model [1] and how it leads to the action for the gauge field in Eq. (3) and its coupling to fermions in Eq. (5). The central insight of HLR is to attach two flux quanta of a U(1) gauge field  $\vec{a}$  to each electron, which creates a composite fermion (CF) denoted by the field  $\psi(\vec{r})$ , as expressed by the constraint

$$\vec{\nabla} \times \vec{a}(\vec{r}) = 2(2\pi)\psi^\dagger(\vec{r})\psi(\vec{r}), \quad (\text{A1})$$

where the CF density on the right-hand side equals the original electron density. An HLR action with  $\tau$  denoting the imaginary time therefore contains a Chern-Simons term for the gauge field  $a_\mu = (ia_\tau, \vec{a})$ , which provides the flux attachment, as is obvious when the  $a_\tau$  component is integrated out to recover Eq. (A1):

$$S_{\text{CF+gauge}} = \int d\tau d^2\vec{x} \psi^\dagger [\partial_\tau - ia_\tau + E(-i\vec{\nabla} + e\vec{A} - \vec{a})] \psi, \quad (\text{A2})$$

$$S_{\text{CS}} = \int d\tau d^2\vec{x} \frac{1}{2(4\pi)} \epsilon_{\mu\nu\lambda} a_\mu \partial_\nu a_\lambda, \quad (\text{A3})$$

where  $\vec{A}$  is the electromagnetic potential and  $E(\vec{k})$  is the electron dispersion. In half-filled Landau levels, the attached  $a_\mu$  gauge flux in the mean-field approximation exactly cancels the external magnetic flux leaving the CF free, however both the fluctuations of  $a_\mu$  and the interactions between the CF

particles cannot be ignored, and it is advantageous to treat them together. The interaction between CF particles is effective and therefore considered to have a varying range,

$$S_{\text{CFint}} = \int d\tau d^2\vec{x} d^2\vec{y} \frac{U}{|\vec{x} - \vec{y}|^{1+\epsilon}} \times \psi^\dagger(\tau, \vec{x}) \psi(\tau, \vec{x}) \psi^\dagger(\tau, \vec{y}) \psi(\tau, \vec{y}), \quad (\text{A4})$$

from Coulomb for  $\epsilon = 0$  to short-range as  $\epsilon \rightarrow 1$ , giving the full HLR action  $S_{\text{HLR}} = S_{\text{CF+gauge}} + S_{\text{CS}} + S_{\text{CFint}}$ . The CF density in the quartic term  $S_{\text{CFint}}$  allows one to rewrite it exactly as a purely gauge field quadratic term using the constraint Eq. (A1), which also implies that only the transverse component of the gauge field  $a_T(\tau, \vec{k}) \equiv (\hat{z} \times \hat{k}) \cdot \vec{a}(\tau, \vec{k})$  at momentum  $\vec{k}$  appears:

$$S'_{\text{CFint}} = \int d\tau d^2\vec{k} \frac{U}{|\vec{k}|^{1-\epsilon}} \frac{1}{(4\pi)^2} |\vec{k}|^2 a_T(\tau, \vec{k}) a_T(\tau, -\vec{k}), \quad (\text{A5})$$

where we dropped an  $\epsilon$ -dependent normalization to obtain the term in our action Eq. (3), where  $a_T$  is relabeled to  $\phi_{j,g}$  after restriction of its momenta determined by patch-pair  $j$  [below Eq. (7)]. Through the transformation from  $S_{\text{CFint}}$  to  $S'_{\text{CFint}}$ , it was recognized that a non-Fermi-liquid fixed point can be accessed in a perturbative expansion of  $\epsilon$  [50].

The CFs couple strongly to the transverse gauge component  $a_T$  due to the scaling transformation [Eq. (7)], which is chosen to preserve the Fermi surface at patch-pairs  $j$  as they scale toward the Fermi point  $\pm \vec{k}_{F,j} = \pm k_F \hat{x}_j$  [49]. Since for a circular Fermi surface the CF current in patch  $j$  gets directed along the  $x$  axis, the expansion of the CF-gauge coupling term  $S_{\text{CF+gauge}}$  in Eq. (A2) has the lowest-order term in powers of gauge field and derivatives  $v_F a_{x_j} (\psi_j^{+\dagger} \psi_j^+ - \psi_j^{-\dagger} \psi_j^-)$  (note that the fermion species index is suppressed). On the other hand, the patches scale such that their aspect ratio remains  $\Lambda_{x_j} \sim \Lambda_{y_j}^2/k_F \ll \Lambda_{y_j}$  [see below Eq. (7)] so that in the RG transformation of patch-pair  $j$  the relevant high-energy gauge modes have momenta  $q_{x_j} \ll q_{y_j}$ . Therefore, in every patch-pair  $j$  the gauge component that couples dominantly to CFs is transverse, i.e.,  $a_{x_j}$  with momentum  $q_{y_j}$ .

### APPENDIX B: RG DIAGRAM FOR $\epsilon_g = \epsilon_\eta$

In this situation, the flow equations (11) lead to flow along rays through the origin:

$$\frac{\eta}{g} = \frac{\eta_0}{g_0}, \quad (\text{B1})$$

and there is a line of fixed points  $(g_*, \eta_*)$  satisfying

$$g_* + \eta_* = \epsilon_*, \quad (\text{B2})$$

where we defined  $\epsilon_* \equiv N\epsilon_g/2 = N\epsilon_\eta/2$ .

On the NQCL, the pairing function  $f(l)$  changes from  $\eta_0 - g_0$  to  $(\eta_0 - g_0) \frac{\epsilon_*}{\eta_0 + g_0}$ , so there is an infinitesimal pairing instability only for  $\eta_0 > g_0$ . Right at the line  $\eta_0 = g_0$  there is BCS behavior that is not expected to be generic beyond one loop.

The NFL energy scale dominates over the pairing scale inside the strip  $\eta_0 - g_0 \ll (\eta_0 - g_0)^2$  in the  $\eta_0 > g_0$  region,

while the converse is found for  $\eta_0 - g_0 \gg (\eta_0 - g_0)^2$  (see Appendix E).

### APPENDIX C: PAIRING FOR $\epsilon_g < \epsilon_\eta$

We can find analytic approximations for the flow of pairing in the limit of  $g_*$  and  $\eta_*$  being similar:

$$|\delta_*| \ll g_*, \quad \text{where } \delta_* \equiv \eta_* - g_*. \quad (\text{C1})$$

This limit is generally convenient as it provides a separation of scales in the RG flow of fermion-boson couplings: the flow of  $(g, \eta)$  is near  $(g_0, \eta_0)$  for  $l \ll 1/\eta_*$ , near the line in Eq. (B2) for  $1/\eta_* \ll l \ll 1/|\delta_*|$ , and near the fixed point for  $l \gg 1/|\delta_*|$ . The separation of scales follows from the analytic solution of RG flow for fermion-boson couplings  $g, \eta$  on the NQCL:

$$\eta(l) = \frac{\eta_0 \exp(\eta_* l)}{1 + h(l) - h(0)}, \quad h(l) = \frac{\eta_0}{\eta_*} e^{\eta_* l} + \frac{g_0}{g_*} e^{g_* l}. \quad (\text{C2})$$

For the case  $g_* < \eta_*$ , we identify several regimes for the pairing gap scale in the region  $\eta_0 < \eta_*$ . With the separation of scales, the  $f(l)$  remains approximately constant for scales  $l \ll 1/\eta_*$ , and in the least favorable case for pairing,  $\eta_0 \ll g_0$ , the value is  $f(l) \approx -g_0$ . It is useful to analyze in general the flow of pairing  $v$  [Eq. (11)] when  $f(l)$  is constant. The outcome is strongly dependent on the sign of the constant. For  $f(l) = -D^2$ ,  $D > 0$ , the flow is

$$v_D(l) = D \frac{v_{\text{init}} + D + (v_{\text{init}} - D) \exp(-2Dl)}{v_{\text{init}} + D - (v_{\text{init}} - D) \exp(-2Dl)}, \quad (\text{C3})$$

with an attractive fixed point at  $v_{\text{init}} = D$  and a repulsive one at  $v_{\text{init}} = -D$ . Only if  $v_{\text{init}} < -D$  is there a pairing instability

$$h(x, y, c) \equiv \frac{\sqrt{x} \text{C}\Gamma(1 - 2\sqrt{y}) [J_{-2\sqrt{y}-1}(2\sqrt{x}) - J_{1-2\sqrt{y}}(2\sqrt{x})] + \Gamma(2\sqrt{y} + 1) (J_{2\sqrt{y}-1}(2\sqrt{x}) - J_{2\sqrt{y}+1}(2\sqrt{x}))}{2 \text{C}\Gamma(1 - 2\sqrt{y}) J_{-2\sqrt{y}}(2\sqrt{x}) + \Gamma(2\sqrt{y} + 1) J_{2\sqrt{y}}(2\sqrt{x})}. \quad (\text{C8})$$

The integration constant  $C$  is fixed by initial conditions  $v(0) = 0$ ,  $\bar{f}(0) = a$ , giving  $h(a/k^2, b/k^2, C) \equiv 0$ , which is easily solved to obtain the parameter-dependent value  $C(a/k^2, b/k^2)$ . Labeling the denominator of  $h$  in Eq. (C8) by  $\chi$ , the pairing instability  $v \rightarrow -\infty$  occurs at scale  $l_P$  when  $\chi \equiv 0$ , which gives the implicit equation

$$\chi \left( \frac{a}{k^2} e^{kl_P}, \frac{b}{k^2}, C \left( \frac{a}{k^2}, \frac{b}{k^2} \right) \right) = 0. \quad (\text{C9})$$

We write  $l_P$  in the form

$$l_P \equiv \frac{1}{k} \ln \left( \frac{k^2}{a} z_P \right), \quad (\text{C10})$$

where  $z_P$  depends in principle on  $a, b, k$ . This corresponds to saying that  $\bar{f}(l_P) \simeq 1$ .

We numerically find that  $z_P$  itself depends very weakly on the parameters and is practically constant of order 1 up to  $a/k^2, b/k^2 \lesssim 0.1$  (see Fig. 5).

$v \rightarrow -\infty$  reached at  $l_{-D} = \frac{1}{2D} \ln \left( \frac{D+|v_{\text{init}}|}{D-|v_{\text{init}}|} \right)$ . Therefore, the pairing interaction  $v$  in the beginning part of the flow ( $l \ll 1/\eta_*$ ) settles at the repulsive value  $v_+ = +\sqrt{g_0}$  (we assume  $v_0 = 0$ ). At the scale

$$l_T = \frac{1}{|\delta_*|} \ln \left( \frac{g_0}{\eta_0} \right), \quad (\text{C4})$$

$f(l)$  becomes positive, and most of the ensuing flow has  $f(l) \approx \eta_*$ . So here we can use the solution to the flow with  $f(l)$  being positive and constant, and the initial condition being  $v_{\text{init}} = v_+ = +\sqrt{g_0}$ . The solution to the flow of  $v$  given  $f(l) = C^2$ ,  $C > 0$ , is

$$v_C(l) = C \tan[-Cl + \arctan(v_{\text{init}}/C)], \quad (\text{C5})$$

with pairing instability  $v \rightarrow -\infty$  reached at  $l_{C+} = \frac{\pi}{C}$  for  $v_{\text{init}} \gg C$ , at  $l_{C-} = \frac{1}{|v_{\text{init}}|}$  for  $v_{\text{init}} \ll -C$  (weak-coupling BCS case), and at  $l_{C0} = \frac{\pi}{2C}$  for  $|v_{\text{init}}| \ll C$ . [Note that drastically different from Eq. (C3), there is always a pairing instability.] Applying Eq. (C5), therefore, gives for the unfavorable case  $g_0 \gg \eta_*$  the pairing scale  $l'_P = \pi/\sqrt{\eta_*}$ . The total pairing scale is then  $l_T + l'_P$ , leading to Eq. (13).

To estimate the pairing scale when the gauge-fermion bare coupling diminishes, for example when  $(g_0, \eta_0)$  is close to the unstable fixed point  $(g_*, 0)$ , we solve a differential equation obtained in various approximations to the flow equation of  $v$  [Eq. (11)]. Let us consider the function  $f$  of the form

$$f(l) \equiv a \exp(kl) - b, \quad (\text{C6})$$

with  $a, b, k$  positive constants. With the substitutions  $v(l) = v(l)/k$ ,  $\bar{f}(l) = (1/k^2)[f(l) + b]$ , we obtain the flow equation

$$\bar{f} \frac{d\bar{v}}{d\bar{f}} = -(\bar{v}^2 + \bar{f} - b/k^2). \quad (\text{C7})$$

The solution takes the functional form  $\bar{v} = h(\bar{f}, b/k^2, C)$ , with

Returning to the physical problem of intermediate and weak bare fermion-gauge coupling, which is still much stronger than bare fermion-nematic coupling, on the NQCL the function  $f(l)$  can in general be rewritten to emphasize the dependence on  $\delta_*$ :

$$f(l) = \frac{\eta_0 \frac{g_*}{g_0} \exp(\delta_* l) - g_*}{1 + X \exp(-g_* l) + \frac{g_* \eta_0}{g_0 \eta_*} \exp(\delta_* l)}, \quad (\text{C11})$$

$$X \equiv \frac{g_*}{g_0} \left( 1 - \frac{\eta_0}{\eta_*} - \frac{g_0}{g_*} \right),$$

where  $X$  measures the distance from the line connecting the fixed points [see Eq. (B2)]. The flow of  $v$  becomes analytically tractable when  $f$  reduces to the form in Eq. (C6). We can therefore consider the example case of  $(g_0, \eta_0)$  close to the unstable fixed point  $(g_*, 0)$  by its behavior on the line  $X = 0$ . Here the denominator of  $f$  is approximately 1 on scales  $l \ll l_v \equiv (1/\delta_*) \ln(\eta_*/\eta_0 - 1)$ . Using  $X = 0$  to eliminate  $g_*/g_0$ ,

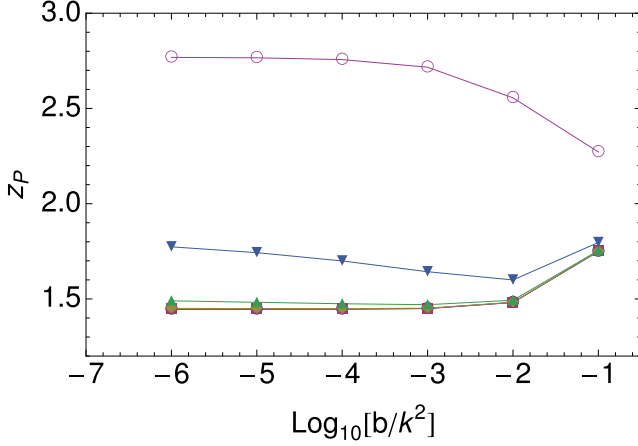


FIG. 5. Pairing the scale factor  $z_P$  [Eq. (C10)] dependence on the parameters  $a/k^2$  and  $b/k^2$  [Eq. (C6)]. The curves from bottom to top are for  $a/k^2 = 10^{-6}, 10^{-5}, \dots, 10^{-1}$ .

we have the tractable form  $f(l) \approx \frac{\eta_0}{1-\eta_0/\eta_*} \exp(\delta_* l) - g_*$ . The consistency condition  $l_P \ll l_v$  reduces to  $\eta_0/\eta_* \ll 1$ . Using this, the result  $l_P = (1/\delta_*) \ln(\delta_*^2/\eta_0)$  follows from Eq. (C10) and the pairing gap is

$$\Delta_P \sim \left( \frac{\eta_0}{\delta_*^2} \right)^{1/\delta_*}. \quad (\text{C12})$$

Next we consider an even weaker gauge-fermion bare coupling  $g_0$ , more precisely the regime  $\frac{\eta_0}{\eta_*} - \frac{g_0}{g_*} \ll 1$ , further assuming that  $l_P \ll 1/\delta_*$ , which makes the numerator of  $f(l)$  constant and the  $X$  term in the denominator dominant [see Eq. (C11)]. The result  $l_P = (1/g_*) \ln[g_*^2/(\eta_0 - g_0)]$  follows, under the constraint  $\eta_0 > g_0$  and  $l_P \ll 1/\delta_*$ . The latter condition can be rewritten as  $\eta_0/\eta_* + g_0/g_* \ll 1$  and  $\eta_0 - g_0 \gg g_*^2 \exp(-g_*/\delta_*)$ , while the gap becomes a stronger power law:

$$\Delta_P \sim \left( \frac{\eta_0 - g_0}{\eta_*^2} \right)^{1/\eta_*}. \quad (\text{C13})$$

Finally, we note that setting  $g_* \ll \eta_*$ , i.e., considering a phase diagram far from the case in Eq. (C1), one expects the results to reduce to the ones in Ref. [42] having fermion-nematic coupling only. In the  $\eta_0 \ll \eta_*$  region of the phase diagram, this is indeed true. Taking  $\eta_0 \ll \eta_*$  in three regimes  $g_0 \ll g_* \ll \eta_*$ ,  $g_0 = g_* \ll \eta_*$ , and  $g_* \ll g_0 \ll \eta_*$ , we find that

$$f(l) \approx \eta_0 \exp(\eta_* l) - g_0, \quad (\text{C14})$$

which leads to the result  $l_P = (1/\eta_*) \ln[(\eta_*^2/\eta_0)]$ , due to  $z_P \approx 1$  [see (C10)].

#### APPENDIX D: PAIRING TRANSITION LINE FOR $\epsilon_g > \epsilon_\eta$

To derive the expression for the pairing transition line in the plane of boson-fermion couplings, we focus on the region  $\eta_0 > g_0$ . Assuming the separation of scales [see Eq. (C1)], we can approximately replace the  $f(l)$  by the positive constant  $\eta_0 - g_0$  in the first part of the flow, and the negative constant  $-g_*$  in the second part of the flow. The vanishing pairing gap at the transition line implies that the pairing scale found in the second part of flow is  $l'_P \rightarrow \infty$ , which is a condition we use

to connect the solutions in the two parts of the flow. The  $f(l)$  becomes negative at

$$l_T = \frac{1}{|\delta_*|} \ln \left( \frac{\eta_0}{g_0} \right), \quad (\text{D1})$$

and once it does it quickly approaches the constant value  $f = -g_*$ . We can use this in the solution of Eq. (C3) for the second part of the flow, except that the initial condition  $v_{\text{init}}$ , being the value of  $v$  when the flow entered the regime  $f \approx -g_*$ , is still unknown. Our demand that  $l'_P \rightarrow \infty$  occurs if  $v_{\text{init}}$  is just below  $-\sqrt{g_*}$  [see Eq. (C3)]. So we can set  $v_{\text{init}} \equiv -\sqrt{g_*}$ , and we use this as a condition for the first part of the flow. The  $v_{\text{init}}$  can be estimated as the value  $v(l_T)$ , while the latter can be estimated by using the first part of the flow, where  $f \approx \eta_0 - g_0 \equiv C^2$ . Using Eq. (C5), therefore, gives the implicit equation that corresponds to the vanishing pairing gap:

$$v_C(l_T) \equiv -\sqrt{g_*}. \quad (\text{D2})$$

Assuming  $Cl_T \ll 1$ , the tangent can be approximated and Eq. (D2) gives Eq. (14) of the main text, which is consistent with  $Cl_T \ll 1$  as long as  $g_0, \eta_0$  are not orders of magnitude larger than the values of  $g_*, \eta_*$ .

We tested the prediction in Eq. (14) by numerically solving the flow; see Fig. 6(a). There is good agreement in the considered regime  $|\delta_*| \ll g_*$ ,  $g_0, \eta_0 \ll g_*$ , however we note that there is excellent agreement with the line

$$\sqrt{\eta_0 - g_0} \ln \left( \frac{\eta_0}{g_0} \right) = \pi |\delta_*| / 2 \quad (\text{D3})$$

in a wider parameter range. This is a noteworthy property of the numerical experiment: it is challenging to numerically observe a divergence  $v(l) \rightarrow -\infty$  at large values of  $l \equiv l_P$ . Deep in the considered regime  $|\delta_*| \ll g_*$ ,  $g_0, \eta_0 \ll g_*$  we could identify flows where  $v$  upon entering into the second part of the flow [see before Eq. (D1)] hovers at a fixed negative value for long stretches of  $l$  before diverging. This is precisely the expected behavior in the approximation of  $f(l)$  being constant in two parts of the flow, in which case  $v$  in the second part starts out just below its unstable fixed point  $-\sqrt{g_*}$ . However, with a given numerical precision and a wider range of initial conditions, it becomes hard to tune  $g_0, \eta_0$  such that this second part of the flow of  $v$  is realized. Instead, one easily identifies the values  $g_0, \eta_0$  for which  $v(l)$  develops a divergence at a relatively small  $l \equiv l_P$  while  $f(l)$  is still not too negative and therefore  $l$  is close to the value  $l_T$  where  $f(l)$  changes sign. That kind of numerical identification of the transition point corresponds to equating  $l_P$  with  $l_T$ . Identifying  $l_P = \pi/(2\sqrt{\eta_0 - g_0})$ , which is a particularly good approximation for slower flows when  $\eta_0, g_0$  are comparable to  $\eta_*, g_*$ , the quoted expression Eq. (D3) follows directly. Of course,  $l_T$  is finite so the condition  $l_P = l_T$  in principle does not allow  $l_P \rightarrow \infty$  and  $\Delta_P \rightarrow 0$ . However, the similarity of curves in Fig. 6(a) shows that the error in our numerical identification of  $l_P$  is small.

The pairing energy scale in the main text is determined using the total pairing scale  $l_T + l'_P$ .

#### APPENDIX E: FLOW OF FERMI VELOCITY

The Fermi velocity flows to zero for any nonzero bare fermion-boson couplings [see Eq. (11)], but it does so in

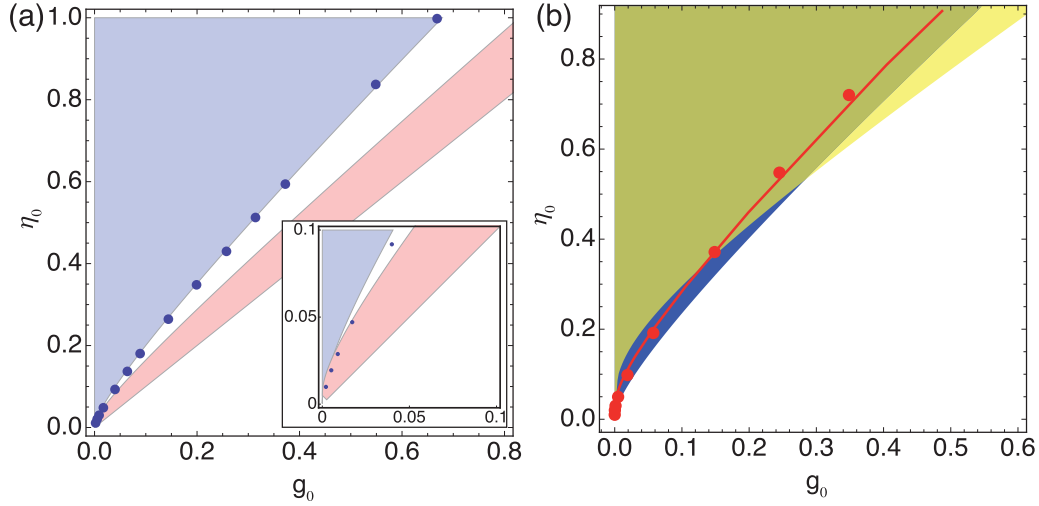


FIG. 6. Line of continuous transition to the paired state in the plane of bare couplings  $(g_0, \eta_0)$  for  $\epsilon_g > \epsilon_\eta$ . (a) On the NQCL, with  $g_* = 1.3, \eta_* = 0.9$ . Blue dots are obtained from numerical solutions to RG flow by having the  $v(l)$  coupling diverge near the largest available scale  $l$ . The boundary of the blue shading is the approximate expression Eq. (D3), and the upper boundary of the red shading is Eq. (14); see the discussion in Appendix D. Inset: zoom-in at small bare couplings. (b) Away from the NQCL,  $R_0 = 0.05$ , and  $g_* = 1.3, \eta_* = 0.8$ . Red dots are obtained from numerical solutions to RG flow by having the  $v(l)$  coupling diverge near the largest available scale  $l$ . The red line is obtained by equating  $l_T'$  [the scale at which the pairing function  $f(l)$  starts repressing the pairing tendency], obtained numerically from Eq. (F3), to the approximation  $l_P = \pi/(2\sqrt{\eta_0 - g_0})$  (see the discussion in Appendix D). The boundary of the blue and yellow shadings uses the two approximate expressions for  $l_T'$  in Eq. (F4), respectively. Note that blue corresponds to  $l_T$  with  $R_0 = 0$ , while yellow matches the slope near the origin better.

different ways depending on the bare couplings  $(g_0, \eta_0)$ . We seek to identify two opposite regimes: (i) the “NFL-dominated” regime where the typical NFL energy scale is much larger than the pairing gap energy, and (ii) the “pairing-dominated” regime where the converse is true. The former case indicates [42] that NFL behavior is observable at temperatures above the pairing (FQH) critical temperature. The typical NFL energy scale can be estimated as  $E \sim \exp(-l_F)$  with  $l_F$  the RG scale at which the Fermi velocity decays. In general, the flow of  $v_F$  [Eq. (11)] is given by  $v_F/v_{F0} = \exp[-I_F(l)]$ , where we define

$$I_F(l) \equiv \int_0^l [g(x) + \eta(x)] dx, \quad I_F(l_F) \equiv 1, \quad (\text{E1})$$

so that non-Fermi-liquid effects become appreciable depending on the RG scale  $l_F$ .

In special case  $g_* = \eta_* \equiv \epsilon_*$ , on the NQCL, the exact solution is

$$l_F = \frac{1}{\epsilon_*} \ln \left( 1 + \frac{\epsilon_*(e-1)}{g_0 + \eta_0} \right). \quad (\text{E2})$$

On the line of fixed points, the exact solution for the scale of pairing (which only happens for  $\eta_0 > g_0$ ) is  $l_P = \frac{\pi}{2\sqrt{\eta_0 - g_0}}$ . Given that  $\epsilon_* \ll 1$ , the NFL-dominated regime appears close to the pairing transition at  $\eta_0 = g_0$ , i.e., for  $\eta_0 - g_0 \ll \epsilon_*^2$ , since  $l_P \gg l_F$  and both are  $\gg 1$ . Conversely, the pairing-dominated regime holds for  $\eta_0 - g_0 \gg \epsilon_*^2$ , where nematic coupling is much stronger than gauge coupling.

This analytic argument can be extended to stronger couplings,  $g_0 + \eta_0 \gg \epsilon_*$ , where  $l_P \approx \frac{\pi}{2\sqrt{\eta_0 - g_0}}$ , and the NFL-dominated regime is found for  $\eta_0 - g_0 \gg (g_0 + \eta_0)^2$ , while the pairing-dominated regime is found for  $\eta_0 - g_0 \ll (g_0 + \eta_0)^2$ .

In the more general case  $\delta_* = \eta_* - g_* \neq 0$  on the NQCL we get qualitatively the same results as above, which we use to sketch the dotted area in the  $(g_0, \eta_0)$  plane of Fig. 3 denoting the regime  $E \gg \Delta_P$ . For completeness, the exact expression for the NFL scale here is

$$\frac{g_0}{g_*} e^{g_* l_F} + \frac{\eta_0}{\eta_*} e^{\eta_* l_F} = \frac{g_0}{g_*} + \frac{\eta_0}{\eta_*} + e - 1. \quad (\text{E3})$$

In the limit  $|\delta_*| \ll 1$ , the approximate solution is  $E \sim (1 + \frac{\eta_*}{g_0 + \eta_0})^{-1/\eta_*}$ , qualitatively the same as Eq. (E2).

It is clear from the  $v_F$   $\beta$  equation [Eq. (11)] that the NFL effects are enhanced by the “total” fermion-boson coupling

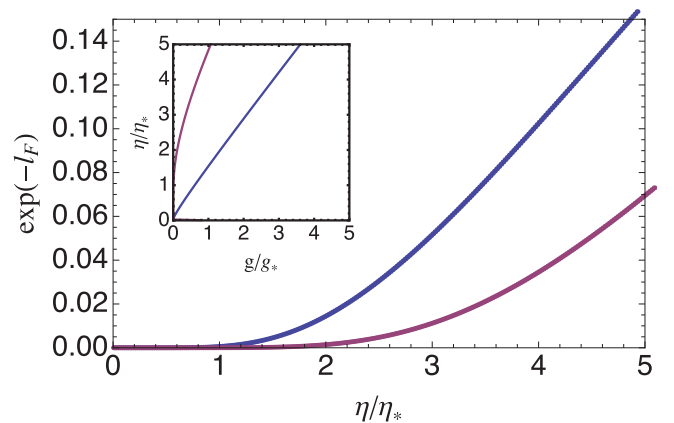


FIG. 7. The NFL energy scale  $\exp(-l_F)$  calculated using Eq. (E3) along two lines in the  $(g_0, \eta_0)$  plane (inset). The bottom line in the inset is the pairing transition line, along which the NFL scale is the top (blue) curve. The top line in the inset gives the bottom (red) line for the NFL scale. The ratio  $g_*/\eta_* = 1.22$ .

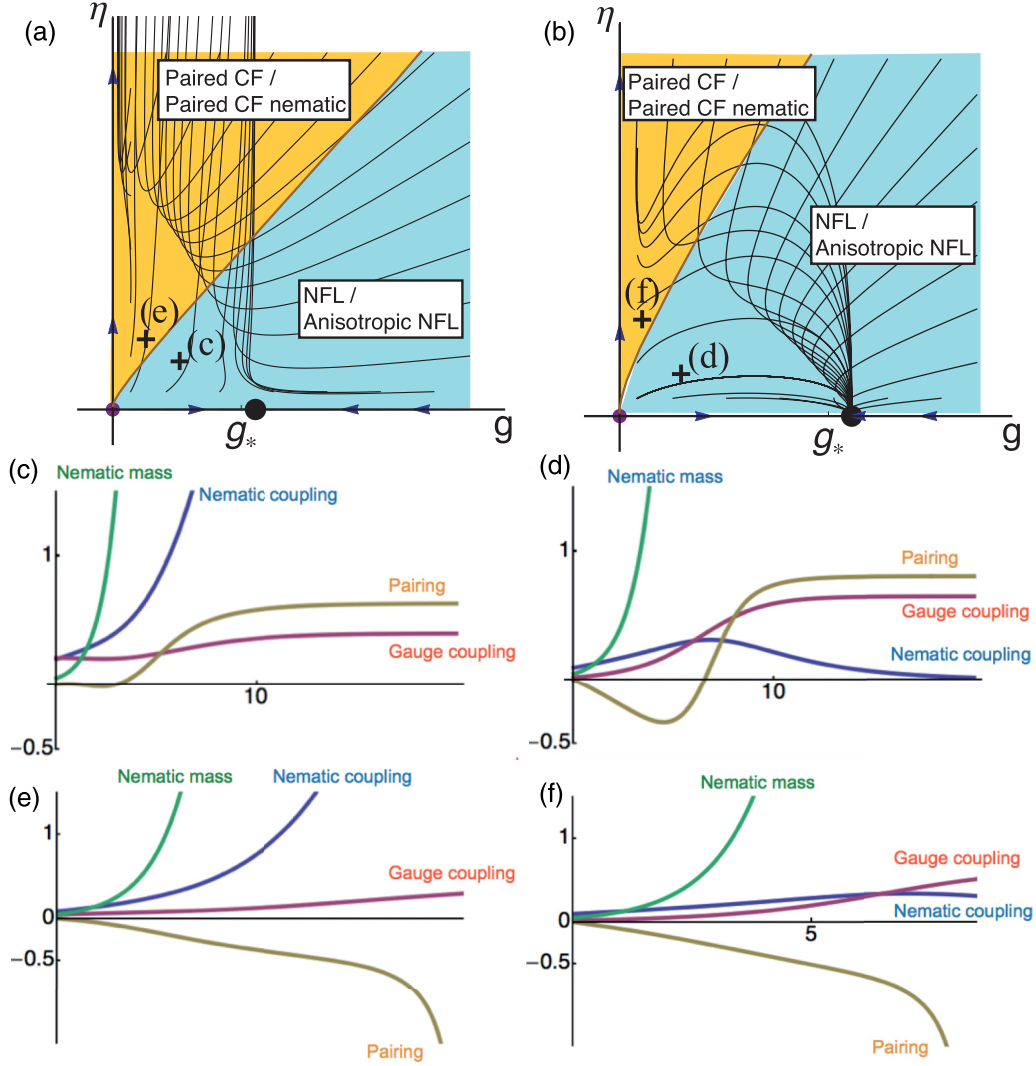


FIG. 8. Numerical RG flows projected onto the fermion-boson coupling plane  $(g, \eta)$  in the vicinity of the NQCL. Colored regions show  $(g_0, \eta_0)$  values, which give states corresponding to the top (bottom) label when  $r_0 > 0$  ( $r_0 < 0$ ). In the orange area there is infinitesimal pairing instability. (a) Case  $\epsilon_g < \epsilon_\eta$  corresponds to Fig. 3(a), with  $R_0/g_* = 0.06$ ,  $g_*/\eta_* = 8/13$ . (b) Case  $g_* > \eta_*$  corresponds to Fig. 3(b), with  $R_0/g_* = 0.008$ ,  $g_*/\eta_* = 13/8$ . Here the topology of RG flows is the same as at the NQCL, except that the unstable fixed point  $(0, \eta_*)$  is replaced by  $(0, \infty)$  affecting flow at  $g = 0$ . (c,d,e,f) Flows of  $g$ ,  $\eta$ ,  $R$ , and pairing  $v$  in (c,e) correspond to initial values marked in panel (a); same for panels (d,f) marked in (b). The horizontal axis is  $\ln l$ .

$g_0 + \eta_0$ . In the unfavorable limit of  $g_0, \eta_0 \rightarrow 0$ , the Fermi velocity takes on a logarithmically slow flow, which makes the RG scale  $l_F$  diverge and the NFL energy scale flat and nearly zero; see Fig. 7.

#### APPENDIX F: FLOW IN VICINITY OF THE NQCL

We define the dimensionless coupling constant  $R \equiv r\kappa_\eta^2/\Lambda_y^{1+\epsilon_\eta}$ , where by  $r > 0$  we label the mass of nematic fluctuations [see Eq. (3)]: if  $r_0 > 0$ , then simply the  $r = r_0$ , while for  $r_0 < 0$  in the vicinity of the nematic transition one has an action for the nematic fluctuations of the same form as Eq. (3), with the bare mass of fluctuations positive at the new minimum and also labeled by variable  $r > 0$ . Since  $R$  is the ratio of the two terms quadratic in the nematic fluctuation field, it is relevant at any fixed point. The coupling of nematic and fermions remains strong near enough to the NQCL, where

dimensionless mass  $rv_F/u_\eta^2\Lambda_y < 1$ . In the case  $R_0 \neq 0$ , exact flows for  $g, \eta$  can be given in integral form (see Fig. 8):

$$\begin{aligned} \eta(l) &= \frac{\eta_0 \exp(\eta_* l)}{1 + p(l) - p(0) + F(l)}, \\ g(l) &= \frac{g_0 \exp(g_* l)}{1 + p(l) - p(0) + F(l)}, \\ p(l) &= \frac{g_0}{g_*} e^{g_* l}, \\ F(l) &= \eta_0 \int_0^l dx \frac{1}{\exp(-\eta_* x) + R_0 \exp(x/2)}. \end{aligned} \quad (F1)$$

For the case  $\epsilon_g < \epsilon_\eta$ , the most important feature of these flows compared to those at the NQCL is that  $F(l)$  replaces a term  $\sim \exp(\eta_* l)$ . Since  $F(l \rightarrow \infty)$  remains finite for any finite  $R_0$ , this implies that the  $\eta$  diverges starting from any nonzero bare

$\eta_0$ . Analytical expressions for the  $F$  can be obtained in limiting cases  $\eta_* = 0$  and 1:

$$F(l, R_0, \eta_* = 0) = l - 2 \ln \left( \frac{1 + R_0 \exp(l/2)}{1 + R_0} \right),$$

$$F(l, R_0, \eta_* = 1) = \frac{2}{\sqrt{R_0}} [\arctan(\sqrt{R_0} e^{l/2}) - \arctan(\sqrt{R_0})]$$
(F2)

with behavior

$F(\eta_* = 0, l \rightarrow \infty)$	$F(\eta_* = 1, l \rightarrow \infty)$
$2 \ln(1 + 1/R_0)$	$2/\sqrt{R_0}[\pi/2 - \arctan(\sqrt{R_0})]$
$R_0 \ll 1$	$2  \ln(R_0) $
	$\pi/R_0$

The fixed point  $(0, \eta_*)$ , which is stable at the NQCL in the case  $\epsilon_g < \epsilon_\eta$ , is therefore removed away from the NQCL and replaced by  $(g_*, \infty)$ ; see Fig. 8(a). Even though  $\eta$  diverges, the nematic fluctuations are suppressed by even faster growth of mass  $R$ , so the new fixed point is equivalent to a stable NFL fixed point at  $(g_*, 0)$ . Consequently, a transition line between the paired state and the NFL appears. We now show how the transition line relates to the one for the case  $\epsilon_g > \epsilon_\eta$  shown in Fig. 8(b), and how both lines depend weakly on value  $R_0 \ll 1$  compared to the transition line found at the NQCL in case  $\epsilon_g > \epsilon_\eta$ . Following the simplified argument below Eq. (D3) (Appendix D), the pairing can occur if  $f$  starts out positive (implying  $\eta_0 > g_0$ ) and the pairing RG scale  $l'_T$  is estimated by the scale at which  $f$  changes sign. Setting  $f(l'_T) \equiv 0$ , we get

$$\frac{\eta_0}{g_0} = \exp(-\delta_* l'_T) + R_0 \exp \left[ \left( \frac{1}{2} + g_* \right) l'_T \right]. \quad (\text{F3})$$

In the relevant regime  $\eta_0 > g_0$ , with  $|\delta_*| \ll \eta_*$ , we obtain the following limits when  $\delta_* < 0$  (i.e.,  $\epsilon_g > \epsilon_\eta$ ):

$$l'_T = \begin{cases} \frac{1}{1+g_*} \ln \left( \frac{\eta_0}{R_0 g_0} \right), & R_0 \gg b, \\ \frac{1}{|\delta_*|} \ln \left( \frac{\eta_0}{g_0} \right), & R_0 \ll b, \end{cases} \quad (\text{F4})$$

where we defined  $b \equiv \left( \frac{g_0}{\eta_0} \right)^{(1/2+\eta_*)/|\delta_*|}$ . The latter limit connects to the NQCL and gives the same value for the transition scale [Eq. (D1)], showing a very weak dependence on  $R_0$  in this limit. When  $\epsilon_g < \epsilon_\eta$  (i.e.,  $\delta_* > 0$ ), the limit  $R_0 \ll b$  is the one giving

$$l'_T = \frac{1}{1+g_*} \ln \left( \frac{\eta_0}{R_0 g_0} \right), \quad R_0 \ll b, \quad (\text{F5})$$

so as expected for  $\epsilon_g < \epsilon_\eta$  we find that the transition line exists only away from the NQCL ( $R_0 \neq 0$ ). These analytical results match well with numerical ones [Fig. 6(b)] if one takes into account the caveats of numerical observation of the pairing transition discussed below Eq. (D3) (Appendix D).

Another way of understanding the presence of similar transition line behaviors for both  $\epsilon_g \leq \epsilon_\eta$  in the vicinity of the NQCL is to focus on the general constraints in the pairing function  $f(l)$ . Away from the NQCL, it has the general form in Eq. (10), and in stark contrast to the case  $R \equiv 0$ , where  $f(l \rightarrow \infty) = \eta_* - g_*$ , it always has the limit  $f(l \rightarrow \infty) = -g_* < 0$  (no matter if  $\eta$  diverges or not). So if  $f(0) < 0$ , and  $f(l)$  does not change sign, there is no possibility of a pairing instability. In general, analyzing Eq. (F3) as a function of  $l'_T$ , we can find the number of sign changes, which together with  $f(0) = \eta_0/(1+R_0) - g_0$  and  $f(\infty) = -g_* < 0$  gives a qualitative picture of the pairing function  $f(l)$ . We find that  $f(l)$  changes once from initially positive (promoting attraction) to negative if  $\eta_0/g_0 > 1 + R_0$ . In contrast, it stays always negative if  $\eta_0/g_0 < m$ , where  $0 < m < 1 + R_0$  is the minimum value of the right-hand side of Eq. (F3) as a function of  $l'_T$ . Only when  $\delta_* > R_0(1/2 + g_*)$  does  $m < 1 + R_0$ , creating the possibility for  $m < \eta_0/g_0 < 1 + R_0$ , for which  $f(l)$  starts out and finishes negative, changing sign exactly twice. The limit  $R \rightarrow 0$  is then obviously not universal, since apart from making  $m = 1$ , it also allows values  $f(\infty)$  that are not negative.

- 
- |   |  |
|---|--|
| <p>[1] B. I. Halperin, P. A. Lee, and N. Read, <i>Phys. Rev. B</i> <b>47</b>, 7312 (1993).</p> <p>[2] R. L. Willett, <i>Adv. Phys.</i> <b>46</b>, 447 (1997).</p> <p>[3] R. R. Du, H. L. Stormer, D. C. Tsui, L. N. Pfeiffer, and K. W. West, <i>Phys. Rev. Lett.</i> <b>70</b>, 2944 (1993).</p> <p>[4] R. R. Du, H. L. Stormer, D. C. Tsui, A. S. Yeh, L. N. Pfeiffer, and K. W. West, <i>Phys. Rev. Lett.</i> <b>73</b>, 3274 (1994).</p> <p>[5] B. Blok and X.-G. Wen, <i>Phys. Rev. B</i> <b>42</b>, 8133 (1990).</p> <p>[6] C. Nayak and F. Wilczek, <i>Nucl. Phys. B</i> <b>479</b>, 529 (1996).</p> <p>[7] E. Fradkin, C. Nayak, A. Tsvelik, and F. Wilczek, <i>Nucl. Phys. B</i> <b>516</b>, 704 (1998).</p> <p>[8] R. L. Willett, <i>Rep. Prog. Phys.</i> <b>76</b>, 076501 (2013).</p> <p>[9] R. Willett, J. P. Eisenstein, H. L. Stormer, D. C. Tsui, A. C. Gossard, and J. H. English, <i>Phys. Rev. Lett.</i> <b>59</b>, 1776 (1987).</p> <p>[10] L. Tiemann, G. Gamez, N. Kumada, and K. Muraki, <i>Science</i> <b>335</b>, 828 (2012).</p> <p>[11] G. Moore and N. Read, <i>Nucl. Phys. B</i> <b>360</b>, 362 (1991).</p> <p>[12] M. Greiter, X. G. Wen, and F. Wilczek, <i>Nucl. Phys.</i> <b>374</b>, 567 (1992).</p> | <p>[13] E. Fradkin and S. A. Kivelson, <i>Phys. Rev. B</i> <b>59</b>, 8065 (1999).</p> <p>[14] E. Fradkin, S. A. Kivelson, M. J. Lawler, J. P. Eisenstein, and A. P. Mackenzie, <i>Annu. Rev. Condens. Matter Phys.</i> <b>1</b>, 153 (2010).</p> <p>[15] M. P. Lilly, K. B. Cooper, J. P. Eisenstein, L. N. Pfeiffer, and K. W. West, <i>Phys. Rev. Lett.</i> <b>82</b>, 394 (1999).</p> <p>[16] D. T. Son, <i>Phys. Rev. X</i> <b>5</b>, 031027 (2015).</p> <p>[17] M. A. Metlitski and A. Vishwanath, <i>Phys. Rev. B</i> <b>93</b>, 245151 (2016).</p> <p>[18] C. Wang and T. Senthil, <i>Phys. Rev. B</i> <b>93</b>, 085110 (2016).</p> <p>[19] Y. You, G. Y. Cho, and E. Fradkin, <i>Phys. Rev. X</i> <b>4</b>, 041050 (2014).</p> <p>[20] Y. You, G. Y. Cho, and E. Fradkin, <i>Phys. Rev. B</i> <b>93</b>, 205401 (2016).</p> <p>[21] M. Mulligan, C. Nayak, and S. Kachru, <i>Phys. Rev. B</i> <b>82</b>, 085102 (2010).</p> <p>[22] G. Y. Cho, O. Parrikar, Y. You, R. G. Leigh, and T. L. Hughes, <i>Phys. Rev. B</i> <b>91</b>, 035122 (2015).</p> |
|---|--|

- [23] D. A. Abanin, S. A. Parameswaran, S. A. Kivelson, and S. L. Sondhi, *Phys. Rev. B* **82**, 035428 (2010).
- [24] S. Kachru, M. Mulligan, G. Torroba, and H. Wang, *Phys. Rev. B* **92**, 235105 (2015).
- [25] J.-S. Jeong and K. Park, *Phys. Rev. B* **91**, 195119 (2015).
- [26] M. Barkeshli, M. Mulligan, and M. P. A. Fisher, *Phys. Rev. B* **92**, 165125 (2015).
- [27] G. Y. Cho, Y. You, and E. Fradkin, *Phys. Rev. B* **90**, 115139 (2014).
- [28] C. Nayak, S. H. Simon, A. Stern, M. Freedman, and S. Das Sarma, *Rev. Mod. Phys.* **80**, 1083 (2008).
- [29] E. H. Rezayi and F. D. M. Haldane, *Phys. Rev. Lett.* **84**, 4685 (2000).
- [30] H. Lu, S. Das Sarma, and K. Park, *Phys. Rev. B* **82**, 201303 (2010).
- [31] K. Pakrouski, M. R. Peterson, T. Jolicoeur, V. W. Scarola, C. Nayak, and M. Troyer, *Phys. Rev. X* **5**, 021004 (2015).
- [32] J. K. Jain, *Phys. Rev. B* **41**, 7653 (1990).
- [33] N. E. Bonesteel, *Phys. Rev. Lett.* **82**, 984 (1999).
- [34] Z. Wang, I. Mandal, S. B. Chung, and S. Chakravarty, *Ann. Phys. (N.Y.)* **351**, 727 (2014).
- [35] T. Morinari, *Phys. Rev. Lett.* **81**, 3741 (1998).
- [36] W. Pan, R. R. Du, H. L. Stormer, D. C. Tsui, L. N. Pfeiffer, K. W. Baldwin, and K. W. West, *Phys. Rev. Lett.* **83**, 820 (1999).
- [37] M. P. Lilly, K. B. Cooper, J. P. Eisenstein, L. N. Pfeiffer, and K. W. West, *Phys. Rev. Lett.* **83**, 824 (1999).
- [38] J. Maciejko, B. Hsu, S. A. Kivelson, Y. J. Park, and S. L. Sondhi, *Phys. Rev. B* **88**, 125137 (2013).
- [39] Y. Liu, S. Hasdemir, M. Shayegan, L. N. Pfeiffer, K. W. West, and K. W. Baldwin, *Phys. Rev. B* **88**, 035307 (2013).
- [40] N. Samkharadze, K. A. Schreiber, G. C. Gardner, M. J. Manfra, E. Fradkin, and G. A. Csáthy, *Nat. Phys.* **12**, 191 (2016).
- [41] M. A. Metlitski and S. Sachdev, *Phys. Rev. B* **82**, 075127 (2010).
- [42] M. A. Metlitski, D. F. Mross, S. Sachdev, and T. Senthil, *Phys. Rev. B* **91**, 115111 (2015).
- [43] S. Lederer, Y. Schattner, E. Berg, and S. A. Kivelson, *Phys. Rev. Lett.* **114**, 097001 (2015).
- [44] Y. Schattner, S. Lederer, S. A. Kivelson, and E. Berg, *Phys. Rev. X* **6**, 031028 (2016).
- [45] P. T. Dumitrescu, M. Serbyn, R. T. Scalettar, and A. Vishwanath, *Phys. Rev. B* **94**, 155127 (2016).
- [46] Z.-X. Li, F. Wang, H. Yao, and D.-H. Lee, *Sci. Bull.* **61**, 925 (2016).
- [47] M. Storni, R. H. Morf, and S. Das Sarma, *Phys. Rev. Lett.* **104**, 076803 (2010).
- [48] D. F. Mross, J. McGreevy, H. Liu, and T. Senthil, *Phys. Rev. B* **82**, 045121 (2010).
- [49] J. Polchinski, *Nucl. Phys.* **422**, 617 (1994).
- [50] C. Nayak and F. Wilczek, *Nucl. Phys.* **417**, 359 (1994).
- [51] V. Scarola, K. Park, and J. Jain, *Nature (London)* **406**, 863 (2000).
- [52] I. Mandal and S.-S. Lee, *Phys. Rev. B* **92**, 035141 (2015).
- [53] M. Mulligan, S. Raghu, and M. P. A. Fisher, *Phys. Rev. B* **94**, 075101 (2016).
- [54] M. Levin, B. I. Halperin, and B. Rosenow, *Phys. Rev. Lett.* **99**, 236806 (2007).
- [55] X. Wan and K. Yang, *Phys. Rev. B* **93**, 201303 (2016).